JOURNAL OF COMPUTATIONAL PHYSICS 77, 340–360 (1988)

An Extension of the Biharmonic Boundary Integral Method to Free Surface Flow in Channels

WEN-QIANG LU* AND HSUEH-CHIA CHANG†

Department of Chemical Engineering, University of Houston, Houston, Texas 77004

Received September 10, 1986; revised April 30, 1987

The biharmonic boundary integral solution of two-dimensional creeping flow of an incompressible Newtonian fluid is extended to problems with free surfaces. Iterative construction of the free surface with the normal stress condition is achieved with a shooting method that is most appropriate for thin films and menisci of widely varying curvature. A continuation scheme is also introduced to systematically construct the solution as a function of a given parameter. These new techniques, combined with the known storage and computational advantages of the biharmonic boundary integral method, allow construction of difficult free surfaces. We demonstrate this by solving the Bretherton problem of a two-dimensional air bubble traveling in a channel. Agreement with asymptotic theory and the finite-difference method is shown. Other problems on formation and transport of bubbles in channels are also tackled.

1. INTRODUCTION

The boundary integral method is especially useful for slow flow problems. The ellipticity of the Stokes equation ensures the existence of fundamental solutions which can be used to convert the equation into an integral equation involving boundary integrals. Consequently, only boundary grids need to be constructed in contrast to the finite-difference and finite-element methods which require interior grids. This provides considerable reduction in storage and computational requirements for the same numerical accuracy. For example, comparative accuracy for two-dimensional problems can be achieved with $O(N)$ grids when finite-difference and finite-element methods require $O(N^2)$ grids. One major difficulty of the method, however, lies in the integration of the fundamental solutions. Earlier applications by Youngren and Acrivos and Rallison and Acrivos [1–3] follow the work of Ladyzhenskaya [4] who constructed the fundamental solutions to the Stokes equation. The integration of the associated singular integrals becomes very

* Present address: Academia Sinica, Beijing, People's Republic of China.

† Present address: Department of Chemical Engineering, University of Notre Dame, Notre Dame, IN 46556.

0021-9991/88 $3.00

tedious in this approach due to the high order singularities of Ladyzhenskaya's fundamental solutions. Lee and Leal [5] and Leal and Lee [6] have carried out meticulous Taylor expansions about the singularities to facilitate the integration. A modified biharmonic boundary integral method which circumvents the integration difficulty has recently been proposed by Kelmanson [7]. By formulating the creeping flow problem in terms of two Laplacian equations of the stream function and the vorticity (see Eq. (1)), his fundamental solutions are simply the low order Laplacian fundamental solution. Consequently, the singular integrals can then be *analytically* evaluated in a piecewise fashion. This represents a significant improvement over the earlier approaches and we shall follow their method in this study.

When a free surface exists in the slow flow problem, the equations are no longer linear due to the interfacial conditions. Nevertheless, by using an iteration scheme which assumes that the profile is known at each step, the problem remains linear at each step and boundary integral methods can still be used [2, 3, 5, 8]. This implies that one of the interfacial conditions must be relaxed during each step and the same condition is then utilized to update the profile in an interative scheme such as the Newton–Raphson method. The choice of the iterative equation has been studied by Silliman [9] for finite-element methods. He found that the normal stress condition should be used at low capillary numbers (the dimensionless velocity, see Eq. (22)). The same condition has also been used by Orr and Scriven [10] and Lowndnes [11] for finite-element methods. It should be mentioned that Saito and Scriven [24] have proposed an alternative scheme without iteration which appears to avoid convergence difficulties for some problems. However, iteration with the normal stress condition is adopted here since convergence is achieved very rapidly in most of our cases. It is also compatible with the continuation scheme that will be described later.

Implementation of the normal stress condition during the iteration step, however, is not a simple matter. Traditionally, this is achieved by collocating the free surface and updating the surface position using a Newton–Raphson scheme until the residual of the normal stress condition converges sufficiently to zero at a finite number of collocation points on the surface [2, 10]. While this method works well on menisci of relatively constant curvature, it usually requires a large number of collocation points for free surfaces with widely varying curvatures. Also, for flat films of very small thickness, local numerical fluctuation often causes the interface to penetrate into impossible regions such as the solid boundary when the above iterative scheme is used. An alternative method is to describe the interface by a prescribed function with unknown parameters which will never exceed the physical region and to estimate these parameters iteratively to minimize the residual. This is the scheme chosen by Kelmanson [8] in his attempt to extend the biharmonic boundary integral method to free-surface flow. However, for surfaces with large changes in the curvature, these prescribed functions usually do not have sufficient degrees of freedom to resolve the interface. In our solution of the Bretherton method, both the collocation technique and the functional description failed.

Instead, we shall propose here an alternative iteration scheme with the normal stress condition. The normal stress condition is converted into a first-order differential equation for the curvature. This differential equation can be formulated in terms of the arclength of the free surface if necessary to improve the resolution. The equation is then solved by a shooting method from one end of the free surface to the other. Prescribed boundary conditions of the curvature at both ends minimize the possibility of erroneous surfaces that exceed the computational domain. For example, in the thin film region, the curvature can be prescribed to be close to zero. More importantly, the shooting method allows arbitrarily fine construction of the free surface by using small and adaptively adjustable shooting step sizes. Steep profiles can be resolved by using the arclength as the independent variable in the differential equation.

A continuation scheme is also utilized in the present analysis. The solutions are traced as functions of the system parameters such as the capillary number, the interfacial pressure drop and the liquid flow rate. The initial guess on the profile for each parameter value is based on the converged profile of the previous value and its derivative. It is similar to the technique used by Chang and Brown [12] for the Rayleigh–Bernard problem. The present problem is especially amenable to this continuation technique. Analytical solutions to the problem are available at some extreme conditions, such as no flow, which can be used to initiate the tracing of the solution branches. In many instances, these continuations allow us to reach problematic profiles which are difficult to construct by iterations using arbitrary initial profiles.

With the combined advantages of the biharmonic boundary integral method, the iteration, and the continuation schemes, we are able to obtain converged two-dimensional profiles of difficult free-surface problems. We will tackle the Bretherton problem of air finger penetration into a channel filled with a viscous fluid [13, 14]. It involves a very thin film of zero curvature which grows into a static cap with curvature equal to the inverse of the half-width of the channel. Hence, it requires resolution of a thin film region and a meniscus with varying curvature. Moreover, asymptotic results for small penetration velocity exist and numerical results for large Ca have also been obtained by Reinelt and Saffman [15] and Shen and Udell [16]. These results allow verification of the results from the present method. Reinelt and Saffman [15] used a finite-difference scheme coupled to a domain transform technique to resolve the thin film and Shen and Udell used finite-elements. With the storage and computational advantages of biharmonic boundary integral method over the finite-difference and finite-element methods, agreement with their result would then justify the former method as an important technique for free-surface problems. We also solve several related problems on steady transport of finite bubbles and cavitation or formation of bubbles behind an obstacle or at an orifice.

2. FORMULATION

The stream-function-vorticity formulation of the two-dimensional creeping flow equations are

$$\nabla^2\psi = \omega \tag{1a}$$

$$\nabla^2\omega = 0. \tag{1b}$$

Defining the fundamental equations to (1) as

$$\nabla_p^2 G_1(p, q) = \delta(|p-q|), \tag{2a}$$

$$\nabla_p^4 G_2(p, q) = \delta(|p-q|), \tag{2b}$$

yields the two-dimensional fundamental functions

$$G_1(p, q) = \log|p-q| \tag{3a}$$

$$G_2(p, q) = |p-q|^2[\log|p-q| - 1] \tag{3b}$$

Applying Green's theorem in the standard boundary integral formulation, one obtains the governing integral equations over the boundary $\partial\Omega$,

$$\xi(p)\,\psi(p) = \int_{\partial\Omega} \{\psi(q)\,G_{1n}(p, q) - \psi_n(q)\,G_1(p, q) + \tfrac{1}{4}[\omega(q)\,G_{2n}(p, q) - \omega_n(q)\,G_2(p, q)]\}\,dq \tag{4a}$$

$$\xi(p)\,\omega(p) = \int_{\partial\Omega} \{\omega(q)\,G_{1n}(p, q) - \omega_n(q)\,G_1(p, q)\}\,dq, \tag{4b}$$

where subscript n denotes the normal derivatives and $\xi(p)$ is the geometric factor related to the Cauchy principal value of the boundary integrals,

$$\xi(p) = \begin{cases} 0, & p \notin \Omega + \partial\Omega, \\ \alpha, & p \in \partial\Omega, \\ 2\pi, & p \in \Omega, \end{cases} \tag{5}$$

where α is the internal angle (in radians) between the tangents to $\partial\Omega$ on both sides of p.

Giben N grids on $\partial\Omega$, the integrals in Eqs. (4) can be discretized assuming piecewise constant functions. The discretized version can be represented by

$$\mathbf{A}\boldsymbol{\psi} + \mathbf{B}\boldsymbol{\psi}' + \mathbf{C}\boldsymbol{\omega} + D\boldsymbol{\omega}' = \mathbf{0} \tag{6a}$$

$$\mathbf{A}\boldsymbol{\omega} + \mathbf{B}\boldsymbol{\omega}' = \mathbf{0}, \tag{6b}$$

where ψ and ψ' are the vectorized ψ and ψ_n values on the grids and ω and ω' the corresponding ones for ω. The matrices **A**, **B**, **C**, and **D** are defined as

$$A_{ij} = \int_{q \in \partial\Omega_j} \frac{\partial}{\partial n} [\log|q_i - q|] \, dq - \xi_j \delta_{ij} \tag{7a}$$

$$B_{ij} = -\int_{q \in \partial\Omega_j} \log|q_i - q| \, dq \tag{7b}$$

$$C_{ij} = \frac{1}{4} \int_{q \in \partial\Omega_j} \frac{\partial}{\partial n} [|q_i - q|^2 \log|q_i - q| - |q_i - q|^2] \, dq \tag{7c}$$

$$D_{ij} = -\frac{1}{4} \int_{q \in \partial\Omega_j} \{|q_i - q|^2 \log|q_i - q| - |q_i - q|^2\} \, dq, \tag{7d}$$

where $\partial\Omega_j$ is the jth segment between nodes j and $j+1$ and the i nodes are taken to be the midpoint of $\partial\Omega_j$. This selection of grid points yields analytical expressions for the elements of the above matrices. Their formulae are given by Jaswon and Symm [17] and Kelmanson [7]. The diagonal terms A_{ii} are not described by Eq. (7). From, Cauchy's principal value theorem, in can be shown that

$$A_{ii} = \pi - \sum_{j \neq i} (A_{ij} - \xi_j). \tag{8}$$

In many earlier applications of the boundary integral method [18, 19], these singular terms are often neglected with the justification that for sufficiently fine grids, their contributions are negligible. We find that such shortcuts are not valid in our problem. For large number of grids ($N > 50$), the matrices with zero diagonal terms are often numerically singular and even when they are non-singular, the iteration often diverges. It is hence important to include the diagonal terms of Eqs. (8).

Equations (6) represent $2N$ equations for the $4N$ unknowns, ψ, ψ', ω, and ω'. The remaining equations must come from the boundary conditions. Hence, at every grid point, two boundary conditions must be specified. This is, of course, impossible in a free-surface problem since the free surface is unknown. However, since we shall adopt an iterative determination of the free surface, at each iteration the surface is known from the previous step. Hence, two conditions on the free surface must be imposed and the remaining one, the normal stress condition, will be used to update the free surface at each iteration. We specify below the most common boundary conditions: (u and v are the tangential and normal velocities in the stationary coordinate and subscripts t and n are the tangential and normal derivatives):

(a) no-slip at wall boundaries S_w ($u = v = 0$)

$$\psi_t = \psi_n = 0 \tag{9}$$

or

$$\psi_n = 0 \qquad \text{and} \qquad \psi = \text{constant}; \tag{10}$$

(b) Symmetry boundaries S_s $(v = u_n = v_t = 0)$

$$\psi = 0 \qquad \text{and} \qquad \omega = 0; \tag{11}$$

(c) unidirectional flows S_i $(v = 0, u(y)$ specified)

$$\omega(y) \qquad \text{and} \qquad \psi(y) \text{ specified}; \tag{12}$$

(d) free surface S_f

$$\psi = 0 \qquad \text{kinematic condition} \tag{13}$$

$$\omega = -2K\psi_n \qquad \text{tangential stress} \tag{14}$$

$$\frac{1}{Ca} K_t = \omega_n - K\omega + 2\psi_{nss} \qquad \text{normal stress,} \tag{15}$$

where K is the curvature of the free surface and s denoted arclength derivative along the interface, $\psi_{nss} = \psi_{ntt} + K\psi_{nn}$ [8]. Equations (14) and (15) are derived by Kelmanson [8]. It is obvious that the normal stress condition, Eq. (15), cannot be easily used as an additional equations since it introduces a new unknown, ψ_{ntt}. Hence, Eq. (15), is best left as the iteration equation. The remaining boundary conditions then provide the missing $2N$ equations which can be solved simultaneously with Eqs. (6). The equations are linear provided the boundaries are specified and the linear matrix equations can be solved by standard library routines.

The iteration procedure based on the normal stress condition involves the path integral

$$K^{j+1}(y) = K(0) + Ca \int_0^y (\omega_n^j - K^j\omega^j + 2\psi_{nss}^j)(\cos\beta_j)^{-1} \frac{dx_j}{dy}\, dy, \tag{16}$$

where β is the angle the tangent t makes with the horizontal coordinate x,

$$dx/dy = -\cot\beta \tag{17}$$

and $x(y)$ is the interface position. The superscripts and subscripts j in (16) refer to the values of the jth iteration. The inclination angle β at a point on the interface is also related to the local curvature by

$$K = \frac{y''}{[1 + y'^2]^{3/2}} = \frac{d\cos\beta}{y'\,dx} = \frac{d\cos\beta}{dy} \tag{18}$$

Hence, the $j+1$ inclination angle can be evaluated from (16) by

$$\cos \beta_{j+1}(y) = \int_0^y K^{j+1}\, dy + \cos \beta(0) \tag{19}$$

and Eq. (17) can be used to obtain the new profile $x_{j+1}(y)$.

The integration constants $\cos \beta(0)$ and $K(0)$ are either specified due to symmetry and imposed pressure drops at the bubble front or $K(0)$ may be determined from the specified values of K at some other locations, say $x \to \infty$. In the latter case, Eq. (16) is integrated once to specify $K(0)$.It should also be noted that the free surface $x(y)$ may be multi-valued function of y. In such cases, the profile may be better represented by $y(x)$ if it is a single-valued function of x and the chain rule can be used to modify Eqs. (16), (17), and (19). Alternatively, an arclength parameterization of the profile can also be used. This would be the most general formulation and allows resolution of steep profiles with respect to x or y. However, the profiles in the present problems can be constructed by the above equations without recourse to the arclength formulation.

In many cases, we facilitate the convergence of the iteration scheme by introducing a relaxation parameter.

$$K^{j+1} = K^j + \alpha(K^{j-1} - K^j), \tag{20}$$

where α is a parameter between zero and unity and its value can be optimized by trial-and-error.

After the iterations have converged to a certain specified tolerance, a continuation technique is used to initiate the next iteration for a different parameter value. Let $\mathbf{x}$ be the vectorized location of the profile $x(y)$, then the continuation scheme is described by

$$\mathbf{x}|_{\lambda+\Delta\lambda} = \mathbf{x}|_\lambda + \frac{d\mathbf{x}}{d\lambda}\Delta\lambda, \tag{21}$$

where $\mathbf{x}|_{\lambda+\Delta\lambda}$ is the initial guess for the profile at $\lambda+\Delta\lambda$ and $\mathbf{x}|_\lambda$ is the converged profile at λ. The derivative $d\mathbf{x}/d\lambda$ can be evaluated from even earlier converged profiles such as at $\lambda-\Delta\lambda$, etc. The increment on $\Delta\lambda$ is also optimized by checking the number of iterations required at each λ value. Details of our continuation technique can be found in our earlier paper on tracing of time-periodic solutions [20]. Other than improving convergence rate, this continuation scheme also allows systematic approaches to difficult profiles from simple or known profiles at different λ values.

3. The Bretherton Problem

The Bretherton problem of a semi-infinite inviscid bubble penetrating into a channel containing an originally stationary viscous fluid is depicted in Fig. 1.

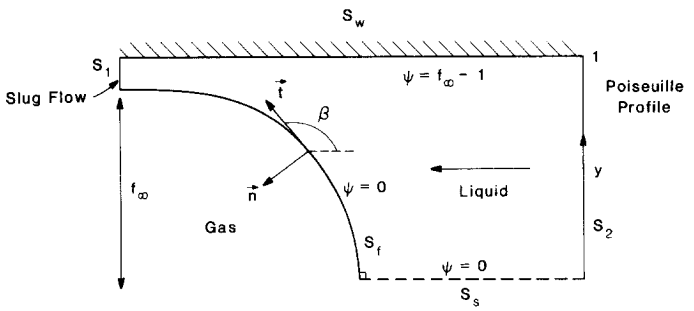

FIG. 1. Schematic for the semi-infinite Bretheron air finger penetration problem.

The lengths are scaled with respect to the half-width of the plates b. The bubble displacement velocity U is used as the characteristic velocity and hence Ca in the normal stress condition of Eq. (15) corresponds to

$$Ca = \mu U/\sigma, \tag{22}$$

where σ is the surface tension coefficient. Pressure is scaled by $\mu U_0/b$. The bubble profile intersects the plane of symmetry S_s at right angles and hence $\cos\beta(0)$ vanishes in Eq. (19). The bubble lays down a stationary film of constant thickness $1-f_\infty$ behind it at $x \to -\infty$ and the liquid flows ahead of the bubble with a Poiseuille profile at $x \to +\infty$. A simple mass balance in the dimensionless variables yields that

$$Q = f_\infty, \tag{23}$$

where Q is the average linear velocity of the liquid upstream in the stationary coordinate. In a coordinate system moving with the steady bubble, the upstream liquid velocity is $Q-1$. Hence, setting ψ to zero on the interface S_f and plane of symmetry S_s, the value of the stream function on the wall becomes $f_\infty - 1$. In this moving reference frame, the tangential velocity of the wall given by (9) must be replaced by

$$\psi_n = -1. \tag{24}$$

The only remaining boundary conditions are the ones at S_1 and S_2. In the moving coordinate, they are

$$\psi = f_\infty - y \qquad \omega = 0 \qquad \text{on} \quad S_1 \tag{25}$$

$$\psi = \frac{3}{2} f_\infty \left(y - \frac{y^3}{3} \right) - y \qquad \omega = -3 f_\infty y \qquad \text{on} \quad S_2. \tag{26}$$

Note that we can just as well specify ψ and ψ_n $(=0)$ on S_1 and S_2 and have the boundary integral method solve for ω and ω_n on these entrance and exit boundaries. At these infinities, the profiles are known exactly and any two of the

TABLE I

Convergence Test of Grid Number N ($Ca = 0.005$)

N	Converged f_∞
62	0.990
67	0.978
77	0.970
82	0.968
87	0.967

variables need to be specified in our approach and the other two will be reproduced in the final result. Finally, during each iteration, $K(0)$ of Eq. (16) is determined by integrating first to $x = -\infty$ to ensure that $K(x = -\infty) = 0$.

Te stationary film left by the bubble decreases in thickness as the bubble velocity diminishes. The Bretherton perturbation result predicts that the two are related by [13]

$$1 - f_\infty = 1.337 Ca^{2/3}. \tag{27}$$

Hence, for Ca values below 10^{-3}, the film is less than 1.5% of the half-width. Numerical analyses which provide such resolution are rare. The only successful attempts are the recent ones by Reinelt and Saffman [15] and Shen and Udell [16]. Reinelt and Saffman only reported results for $Ca > 10^{-2}$ while Shen and Udell's minimum Ca is 5×10^{-3}, although they only consider axisymmetric bubbles. With these results from alternative approaches, this problem is ideal for testing the present biharmonic boundary integral method. More importantly, the validity of Eq. (27) for small Ca will be verified in the present analysis.

The locations of S_1 and S_2 are chosen to be $x = -5$ and $x = +5$, respectively. The results do not change significantly by pushing them further away. Different numbers of equally spaced grids are constructed on the boundaries to determine the number of grids needed for convergence. The result tabulated in Table I for

TABLE II

Grid Points on the Boundaries of Figure 1

S_f	34
S_1	3
S_2	10
S_w	20
S_s	10
Total	77

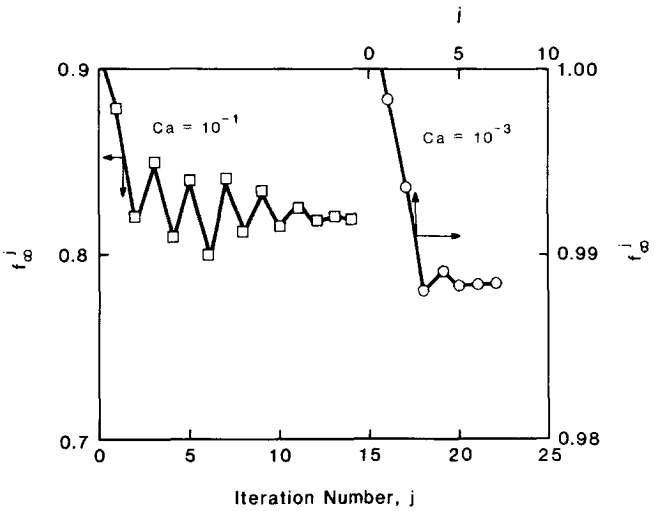

FIG. 2. Iteration history for $Ca = 10^{-1}$ and 10^{-3}.

$Ca = 5.0 \times 10^{-3}$ indicates that grid numbers exceeding 70 yields f_∞ within 0.5% of the converged value which is within 0.6% of Bretherton's asymptotic result of 0.9609. This is compared to $N = 55 \times 34$ in the finite-difference approach for Reinelt and Saffman. The distribution of grids for $N = 77$ in our method is tabulated in Table II. Variation in N in Table I is achieved by adjusting the number of grids on the two unknown boundaries S_f and S_1. Convergence of the iterations for $Ca = 10^{-1}$ and 10^{-3} are depicted in Fig. 2. Tolerance can be achieved up to

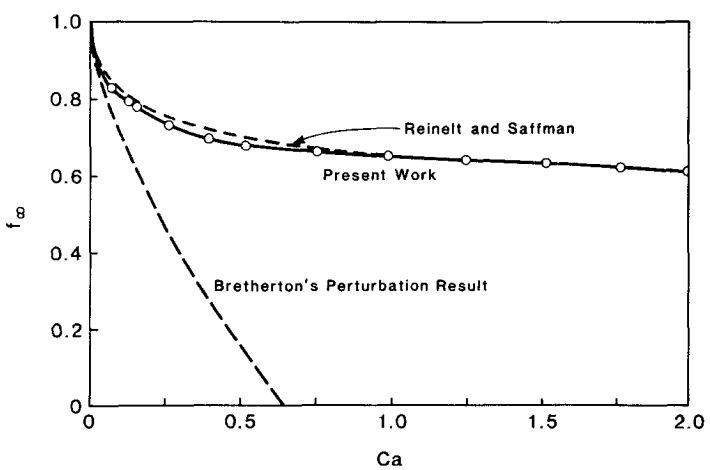

$|f_\infty^{j+1} - f_\infty^j|/f_\infty^j < 10^{-6}$. These iterations are not preceded by the continuation technique of Eq. (21). Nevertheless, the high initial guesses of f_∞ converge rapidly in less than 15 iterations. Each iteration only takes approximately 2 s of CPU on the AS9000. In general, the number of iterations for convergence increases with *Ca*. However, resolution of thin films for small *Ca* is often difficult during integration of Eqs. (16), (17), and (19).

The continuation scheme is initiated at large *Ca* where the film is thick and the profile is more readily obtainable. The solution branch is then traced for decreasing *Ca*. The scheme fails at approximately 5.0×10^{-4} when the film is too thin for the integrations of Eqs. (16), (17), and (19). The large *Ca* results are shown in Fig. 3 and compared to the perturbation result of Bretherton, Eq. (27), and Reinelt and Saffman's finite-difference result. (The numerical data are kindly supplied by D. A. Reinelt). It is clear that the Bretherton perturbation analysis breaks down for $Ca > 10^{-1}$. There is a small difference between our result and Reinelt and Saffman's for *Ca* between 0.1 and 0.8. The small $1 - f_\infty$ ($Ca < 1$) results are shown in Fig. 4 and compared to the Bretherton correlation. Excellent agreement between numerical and perturbation results at low *Ca* is evident. It should also be noted that for $Ca > 10^{-1}$, the numerical results can be described by the correlation

$$1 - f_\infty = 0.35 Ca^{3/20} \tag{28}$$

which can be used to replace Eq. (27) for thick films.

In Fig, 5, we present the pressure drop across the bubble front as a functon of *Ca*. Comparison is made to Reinelt and Saffman and Bretherton's two-dimensional

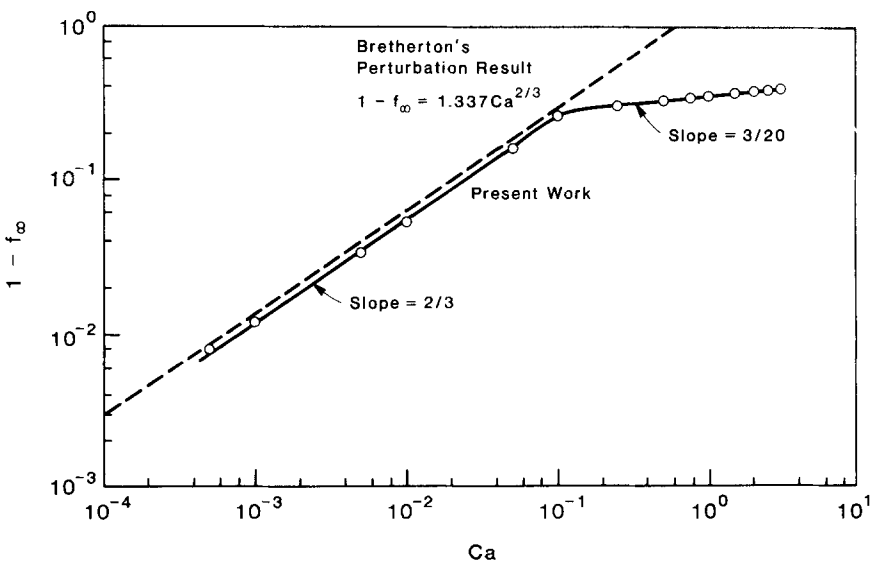

FIG. 4. Comparison of low *Ca* numerical result to Bretherton's perturbation result.

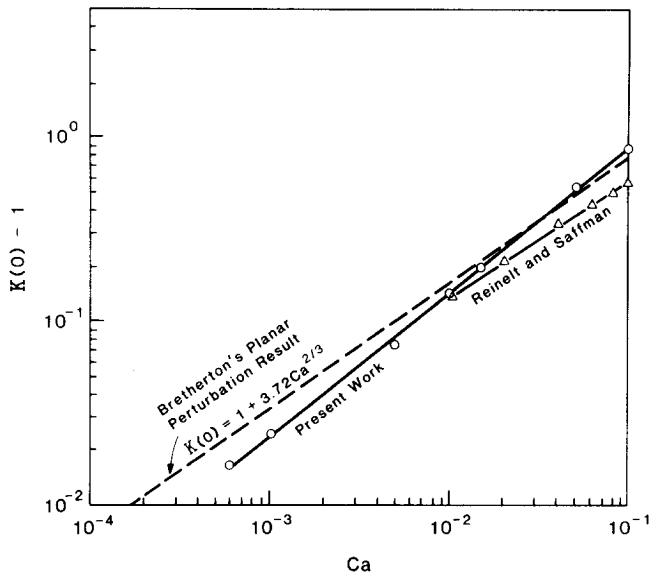

FIG. 5. Comparison of pressure drop correlation of various approaches.

results. The excess pressure is determined from the local curvature at the bubble front and is the least accurate variable due to the derivatives of the profile in Eqs. (17) and (18). Given that, both our result and Reinelt and Saffman's result for larger Ca yield reasonable agreement to the asymptotic theory of Bretherton,

$$\frac{(p_g - p_l)b}{\sigma} = \Delta P\, Ca = K(0) = 1 + 3.72Ca^{2/3}, \tag{29}$$

where ΔP is the dimensionless pressure drop, $(p_g - p_l)b/\mu U_0$. Note that in Bretherton's original derivation [13] for any axisymmetric bubble, the profile is matched to a hemisphere at the tip and the resulting pressure drop is given by $(2\sigma/b)\{1 + 1.79(3\mu U_0/\sigma)^{2/3}\}$. In the present planar case, a half-circle instead of the hemisphere is appropriate and a similar matching analysis removes the factor of 2 for the axisymmetric bubble to yield Eq. (29). It should be emphasized that our technique is able to resolve the tip curvature to a lower Ca than Reinelt and Saffman. This is because the curvature K is solved explicitly in the shooting iterations of Eq. (16). Moreover, we can easily choose step sizes of arbitrarily small magnitude during the shooting to resolve the tip region. In contrast, this is not as easily accomplished with the other methods since one would have to repeatedly construct extremely fine grids or elements in the tip region to achieve comparable accuracy. Also, since the profile position instead of K is computed in the other iteration schemes, $K(0)$ would have to be estimated by taking derivatives of the profile as in Eq. (18). The estimation of the large first and second derivatives at the

tip again reduces the accuracy of previous methods. In our method, the curvature K is obtained directly and explicitly.

By setting the Poiseuille stream function in Eq. (26) to zero, and intermediate location y_0 between S_s and S_w where the stream function changes sign,

$$\psi(y_0)=0, \qquad \frac{\partial\psi}{\partial y}(y_0)\neq 0 \tag{30}$$

is given by

$$y_0^2=\frac{2}{f_\infty}\left[\frac{3}{2}f_\infty-1\right]. \tag{31}$$

Hence, for thin films

$$f_\infty>\tfrac{2}{3} \tag{32}$$

flow separation exists in the upstream Poiseuville flow and an additional stagnation point exists on the bubble other than the tip. This separation occurs for small Ca ($\leqslant 0.125$ from Bretherton's correlation, Eq. (27) and 0.1245 from our numerical result) and reflects a dramatic reversal of flow near the bubble front and at the

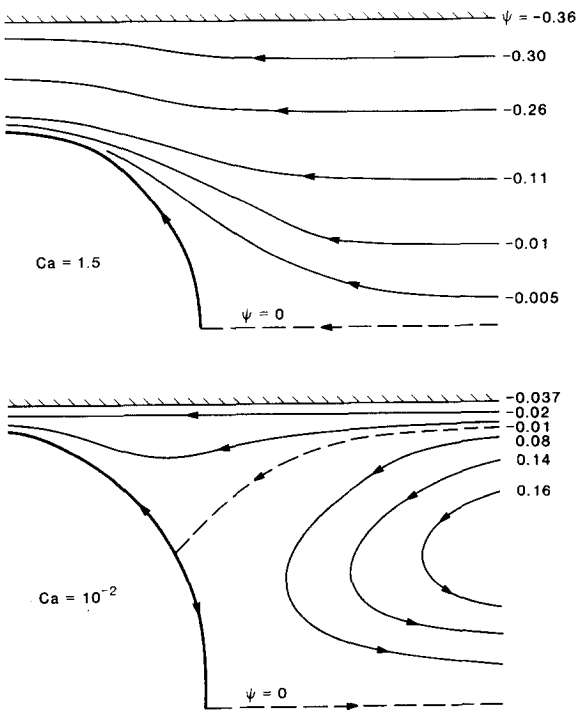

FIG. 6. Streamlines at two different Ca values with flow separation at the lower Ca.

plane of symmetry. The stagnation point on the bubble moves towards the front with increasing Ca until $Ca = 0.125$ according to Eq. (31). Our simulated flow fields for $Ca = 1.5$ and $Ca = 10^{-2}$ are presented in Fig. 6. The existence of the stagnation points implies that only part of the liquid upstream is entrained into the film region. This accounts for the dramatic deviation from the Bretherton solution in Fig. 4 and represented by Eq. (28). Not surprisingly, the deviation begins at approximately $Ca = 0.125$ (see Fig. 4).

4. Bubble Formation at an Orifice

Another important engineering problem of free surface flow in channels is bubble formation (cavitation) at orifices (behind obstacles in a flowing channel) [21]. This is related to studies of aeration, cavitation, boiling, and gas–liquid equipment. Chuang and Goldshmidt [21] have measured the volume (or effective radius) of a bubble that can be sustained stationarily at the orifice. Under constant pressure drop conditions, the steady-state bubble volume decreases sharply with increasing

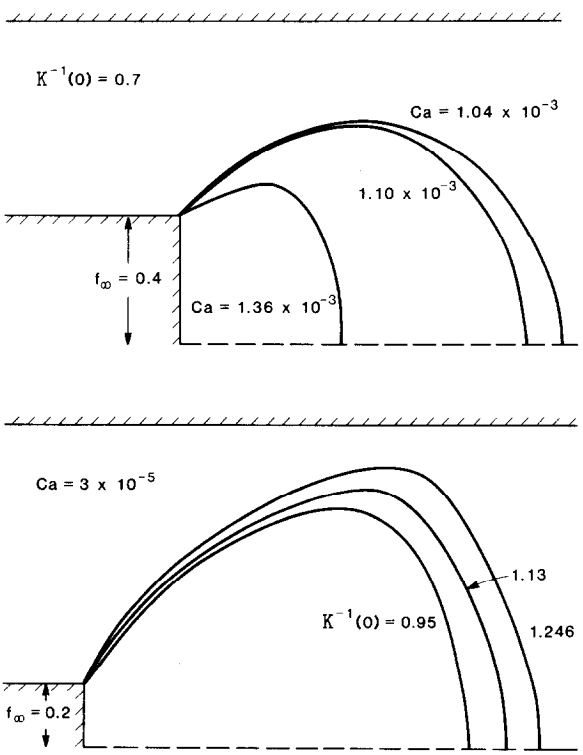

FIG. 7. Bubble profiles at the orifice for various values of liquid flow rate Ca and bubble front pressure drops $K^{-1}(0)$.

liquid flow rate until the bubble is essentially "chocked" by the flow. At constant flow rate conditions, the bubble volume increases with increasing pressure drop as expected. The two-dimensional unbounded potential flow version of this problem has recently been analyze by Vanden-Broeck [22]. We tackle here the Stokes flow limit in a bounded channel with the geometry depicted in Fig. 7. The characteristic velocity is chosen to be Q/b, where Q is half the liquid volumetric flow rate and b the channel half-width. Hence, Ca is now associated with the liquid velocity downstream. Poiseuille profiles are imposed downstream and upstream,

$$S_1: \begin{cases} \psi = \dfrac{6}{(1-f_\infty)^3}\left\{\left[\dfrac{1+f_\infty}{2}\,y^2 - f_\infty\, y - \dfrac{y^3}{3}\right] - \dfrac{(f_\infty^3 - 3f_\infty^2)}{6}\right\} & \text{(33a)} \\ \psi_n = 0 & \text{(33b)} \end{cases}$$

$$S_2: \begin{cases} \psi = \frac{3}{2}(y - y^3/3) & \text{(34a)} \\ \psi_0 = 0. & \text{(34b)} \end{cases}$$

The boundary conditions are

$$\begin{aligned} &\psi = 1 \quad \psi_n = 0 \quad \text{at the wall} \\ &\psi = 0 \quad \psi_n = 0 \quad \text{at the orifice.} \end{aligned} \tag{35}$$

The other boundary conditions are identical to the semi-definite Bretherton

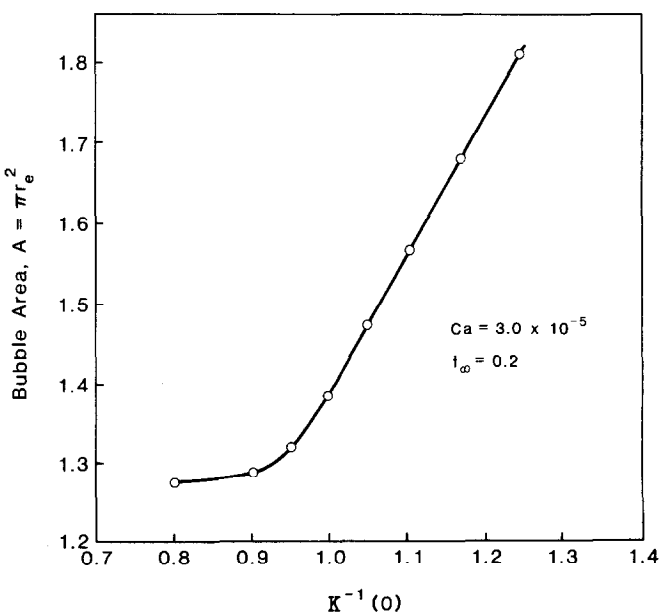

FIG. 8. Numerical results of bubble area dependence on pressure drop at given Ca and orifice size.

problem of previous sections. Note that the surfaces within the bubble are excluded from the problem since we neglect flow of the interior fluid. Consequently, whether the orifice is open or closed is irrelevant and the problem is equally applicable to bubble formation at an orifice or cavitation behind a rectangular obstacle.

We use an iteration trick to greatly simplify the present problem. If one specifies the locations of the bubble front and the orifice edge, $K(0)$ of Eq. (16) is determined and integrations of Eqs. (16), (17), and (19) must be carried out during each iteration (as in the Bretherton problem) to ensure the interface hits the edge and to specify $K(0)$. Instead, we choose to fix $K(0)$ a priori without specifying the location of the orifice edge. Integrations are then initiated from the bubble front until the interface height reaches the orifice height f_∞ from above. This specifies the location of the orifice edge for that iteration. Iterations are then continued until the location of the orifice edge converges. The quantity $K^{-1}(0)$ is the radius of curvature of the bubble front and fixing $K(0)$ is equivalent to specifying the pressure drop across the bubble tip (see Eq. (29)).

The present problem is also most suitable for the solution continuation approach. The bubble profile for $Ca = 0$ just the arc of a circle of radius $K^{-1}(0)$ (see Fig. 7 for small Ca). This can be used to initiate the continuation with respect to Ca. The

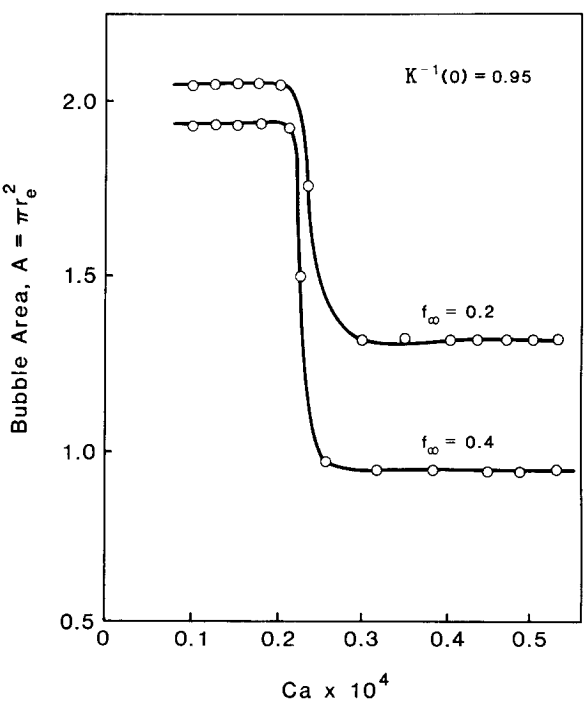

FIG. 9. Numerical results of bubble area dependence on liquid flow rate Ca at given pressure drop and two orifice sizes.

continuation can then be stopped at a certain Ca and continuation with respect to $K(0)$ can be initiated. In this fashion, one can construct profiles with front radius, $K^{-1}(0)$, larger than the unity tube half-width. These profiles are difficult to obtain using arbitrary initial profiles for the iteration. A profile with $K^{-1}(0) = 1.25$ is shown in Fig. 7.

The results are summarized in Figs. 8 and 9 which depict the bubble area (πr_e^2, where r_e is the effective bubble radius) as functions of $K^{-1}(0)$ (inverse tip pressure drop) and Ca (down stream liquid velocity). Drastic drops and increases in bubble area are evident after certain critical values of $K^{-1}(0)$ and Ca.

5. Finite Bubbles

In the original lubrication analysis of Bretherton [13] on steady transport of bubbles, the bubble length is arbitrary and his perturbation results are not length dependent. In fact, his results for the front and back halfs of the bubble are related only by the film thickness in the middle, given by Eq. (27), and are otherwise independent. Moreover, his bubbles are not symmetric with respect to reflection across the middle. In Section 3, we have successively validated his analysis of the front half at small Ca ($< 10^{-1}$). In this section, we study the transport of finite bubbles. We will atempt to verify Bretherton's correlation for pressure drop across a bubble,

$$\Delta K = K_{\text{front}} - K_{\text{back}} = 4.7 Ca^{2/3}. \tag{36}$$

(Again, the original Bretherton result is scaled by a factor of 2 to convert his axisymmetric derivation to the present planar case). However, we shall also investigate cases where the liquid is also flowing at an average linear velocity Q less (< 1) or larger (> 1) than the bubble velocity in the stationary coordinate. The liquid can even flow in the opposite direction from the bubble ($Q < 0$). Unlike the rigid particle case studied by Leichtberg *et al.* [23], the nonlinear free surface conditions of the present problem stipulate that the results for different liquid velocity Q and bubble velocity Ca are not additive. Both parameters need to be specified in all our analysis.

The boundary conditions are identical to the ones in Section 3 on semi-infinite bubbles except that the downstream liquid flow profile is now Poiseuille. However, the iteration procedure is now considerably different. The front curvature $K(0)$ (or K_{front}) is determined during each iteration by stipulating that the back tip is perpendicular to the plane of symmetry, viz. β_e is 90°. This is done by integrating Eqs. (16) and (19) once during each iteration step to determine $K(0)$. In addition, unlike semi-infinite bubbles, the bubble area is now specified,

$$2\int_0^{x_e} y\, dx = A = \pi r_e^2, \tag{37}$$

where x_e is the location of the back tip and r_e is the effective bubble radius. Convergence is determined by the variation in x_e or the maximum of the profile y_m.

Solution of the present finite bubble problem proves to be far more difficult than the previous two. Iterations for y_m close to the f_∞ value of the thin film semi-infinite case invariably diverge. Satisfactory result can only be obtained for $y_m < 0.6$ and only with accuracy of $|y_m^{j+1} - y_m^j|/y_m^j < 10^{-3}$. As is evident from Fig. 4, the Bretherton analysis is not excepted to be valid for such small bubbles. Nevertheless, we present the converged profiles in Fig. 10 and the computed ΔK in Fig. 11 in comparison to Eq. (36). The computed ΔK for $Q = 0$ (stationary film), which corresponds to Bretherton's case, can be approximated by $\Delta K \sim 3.0 Ca^{2/3}$. Hence, the numerical result duplicates the power dependence on Ca of the perturbation result but not the coefficient. It should of course be realized that the perturbation results are for long bubbles with extremely thin liquid layers near the channel wall, a limit that cannot be resolved numerically presently. The streamlines of a more deformed profile is shown in Fig. 12. Note the vortex pair behind the bubble. This flow separation phenomenon seems to occur readily in the present problem despite the absence of intertial (vanishing Reynolds number).

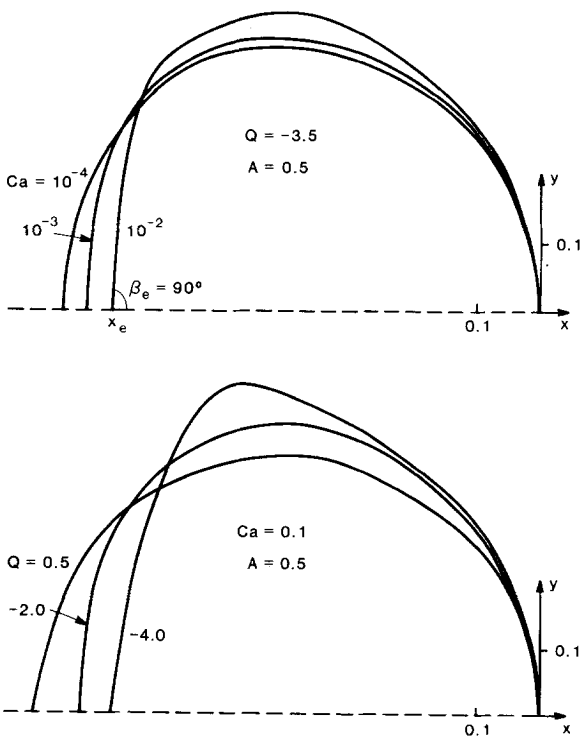

FIG. 10. Bubble profiles of finite bubbles at various bubble velocity Ca and liquid flow rate Q values at given bubble area.

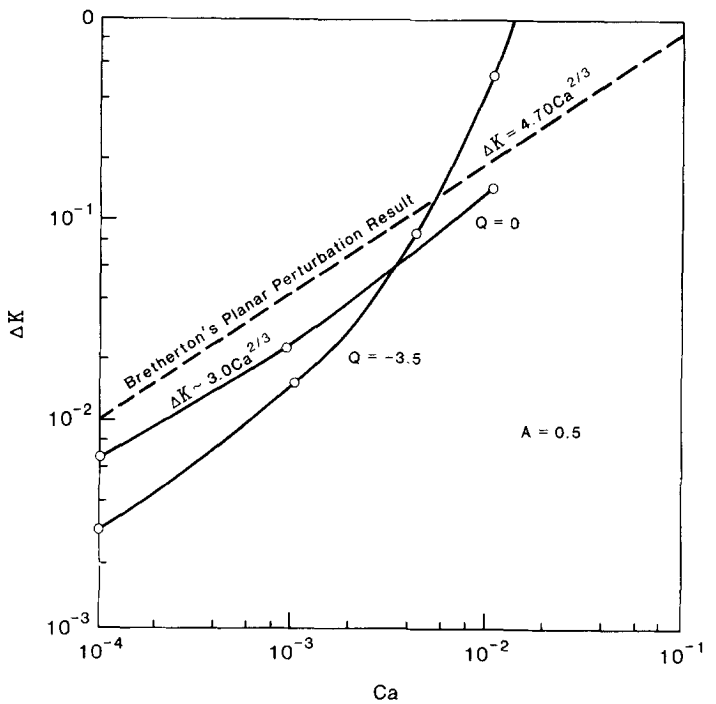

FIG. 11. Pressure drop dependence of a finite bubble of area 0.5 at various Q and Ca values. Bretherton's perturbation result for long bubbles is also depicted.

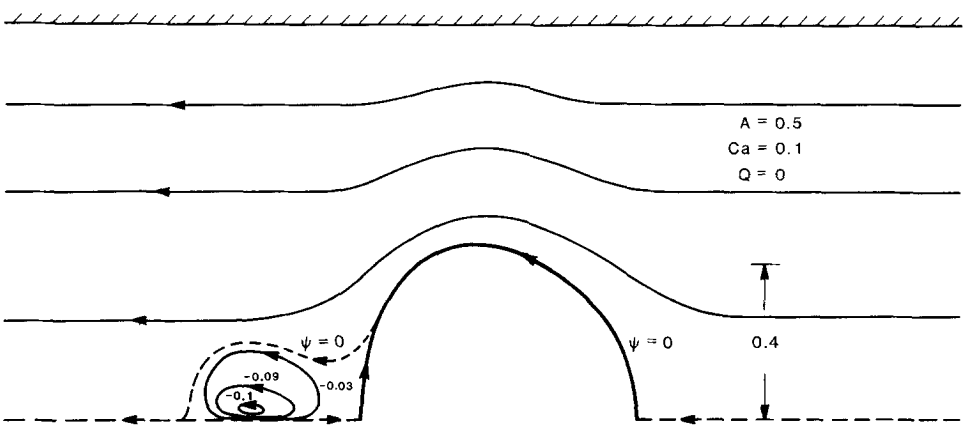

FIG. 12. Streamlines of a finite bubble of area 0.5 penetrating into a stagment fluid ($Ca = 0.1$ and $Q = 0$). Note flow separation behind the bubble.

6. Conclusion

An iterative and continuation scheme has been presented for a biharmonic boundary integral boundary method for steady bubble transport problems in two-dimensional channels filled with viscous fluids. The technique is verified comparison against the asymptotic Bretherton solution for the semi-infinite bubble penetration problem at Ca values lower than those obtained from finite-difference and finite-element methods. It has also constructed bubble profiles and bubble sizes during formation at an orifice or cavitation behind an obstacle. Partial results have been obtained for the steady transport of small bubbles in a channel. The advantages of the present method are not limited to the boundary integral formulation with its obvious superiority in computation and storage capacities. They also include the unique choices of iteration schemes and the use of continuation technique to reach difficult locations in the parameter space. It should be mentioned that asymptotic estimates on the profiles are often used as initial guesses of the iterations, as Kelmanson [8] and Reinelt and Saffman [15] have done. However, in problems where such perturbation analysis is not possible, the continuation scheme presented here is especially advantageous. Even if perturbation results are available, one can use the asymptotic profiles to initiate the continuation scheme and trace the solutions into regions where the asymptotic analysis breaks down. In this fashion, the present numerical scheme is an excellent complement to perturbation analysis for interfacial problems under Stokes flow conditions. Finally, the present method still requires construction of the fundamental solutions. Extension to the axisymmetric problem would be straightforward since the Green's functions for the axisymmetric Laplacian are readily available. For Hele–Shaw problems with lateral curvature as discussed by Park and Homsy [14], however, the Green's functions would not be easy to construct.

Acknowledgment

WQL is grateful for the financial support of the Enhanced Oil Recovery consortium of the University of Houston.

References

1. G. K. Youngren and A. Acrivos, *J. Fluid Mech.* **69** (2), 377 (1975).
2. G. K. Youngren and A. Acrivos, *J. Fluid Mech.* **76** (3), 433 (1976).
3. J. M. Rallison and A. Acrivos, *J. Fluid Mech.* **89** (1), 191 (1978).
4. O. A. Ladyzenskaya, *The Numerical Theory of Viscous Incompressible Flow* (Gordon & Breach, New York, 1963), p. 62.
5. S. H. Lee and L. G. Leal, *J. Colloid Interface Sci.* **87** (1), 81 (1982).
6. L. G. Leal and S. H. Lee, *Adv. Colloid Interface Sci.* **17**, 61 (1982).
7. M. A. Kelmanson, *J. Comput. Phys.* **51**, 139 (1983).
8. M. A. Kelmanson, *J. Eng. Math.* **17**, 329 (1983).

9. W. J. SILLIMAN, "Viscous Film Flow with Contact Lines: Finite Element Simulation, A Basis for Stability Assessment and Design Optimization," Ph.D. thesis, University of Minnesota, 1979 (unpublished).
10. F. M. ORR AND L. E. SCRIVEN, *J. Fluid Mech.* **84**, 145 (1978).
11. J. LOWNDNES, *J. Fluid Mech.* **101** (3), 631 (1980).
12. C. J. CHANG AND R. A. BROWN, *J. Comput. Phys.* **53**, 1 (1984).
13. F. P. BRETHERTON, *J. Fluid Mech.* **10**, 166 (1961).
14. C. W. PARK AND G. M. HOMSY, *J. Fluid Mech.* **139**, 291 (1984).
15. D. A. REINELT AND P. G. SAFFMAN, *SIAM J. Sci. Statist. Comput.* **6**, 542 (1985).
16. E. I. SHEN AND K. S. UDELL, *J. Appl. Mech.* **107**, 253 (1985).
17. M. A. JASWON AND G. T. SYMM, *Integral Equation Methods in Potential Theory and Elastostatics* (Academic Press, New York, 1977).
18. M. MAITI AND S. K. CHAKRABARTY, *Int. J. Eng.* **12**, 793 (1974).
19. Y. S. WU, F. J. RIZZO, D. J. SHIPPY, AND J. A. WAGNER, *Q. Elec. Mach. Electromech.* **1**, 301 (1977).
20. M. ALUKO AND H.-C. CHANG, *Comp. and Chem. Eng.* **8**, 355 (1984).
21. S. C. CHUANG AND V. W. GOLDSCHMIDT, *J. Basic Eng.*, 706 (1970).
22. J.-M. VANDEN-BROECK, *Phys. Fluids* **27** (11), 2601 (1984).
23. S. LEICHTBERG, R. PFEFFER, AND W. WEINBAUM, *Int. J. Multiphase Flow* **3**, 147 (1976).
24. H. SAITO AND L. E. SCRIVEN, *J. Comput. Phys.* **42**, 53 (1981).